CHEMISTRY OF MATERIALS
Cite This: Chem. Mater. 2019, 31, 8957−8968
Article
pubs.acs.org/cm

One Ion, Many Facets: Efficient, Structurally and Thermally Sensitive Luminescence of Eu^{2+} in Binary and Ternary Strontium Borohydride Chlorides

Thomas Wylezich,[†] Atul D. Sontakke,[‡] Victor Castaing,[§] Markus Suta,[‡] Bruno Viana,[§] Andries Meijerink,[‡] and Nathalie Kunkel*[,†,∥]

[†]Chair for Inorganic Chemistry with Focus on Novel Materials, Department of Chemistry, Technical University of Munich, Lichtenbergstr. 4, 85747 Garching, Germany

[‡]Condensed Matter and Interfaces, Debye Institute for Nanomaterials Science, Department of Chemistry, Utrecht University, Princetonplein 1, 3584 CC Utrecht, The Netherlands

[§]Chimie ParisTech, PSL University, CNRS, Institut de Recherche de Chimie Paris, 11 rue Pierre et Marie Curie, 75005 Paris, France

[∥]Institut für Anorganische Chemie, Georg-August-Universität Göttingen, Tammannstrasse 4, 37077 Göttingen, Germany

Supporting Information

ABSTRACT: The Eu^{2+}-doped mixed alkaline metal strontium borohydride chlorides $ASr(BH_4)_{3-x}Cl_x$ (A = K, Rb, Cs) and Eu^{2+}-doped strontium borohydride chloride $Sr(BH_4)_{2-x}Cl_x$ have been prepared by mechanochemical synthesis. Intense blue photoluminescence for $Sr(BH_4)_{2-x}Cl_x$ (λ_{em}= 457 nm) and cyan photoluminescence for the perovskite-type mixed alkaline metal strontium borohydride chlorides $ASr(BH_4)_{3-x}Cl_x$ (A = K, Rb, Cs) (λ_{em} = 490 nm) is already observable after short milling times. Temperature dependent luminescence measurements reveal an appreciable blue shift with increasing temperature for all $ASr(BH_4)_{3-x}Cl_x$ (A = K, Rb, Cs) until 500 K. This extremely large shift, caused by structural relaxation, as well as the vibrationally induced emission band broadening can serve as a sensitive response signal for temperature sensing, and this unique behavior has, to the best of our knowledge, not been reported in any Eu^{2+} doped phosphor so far. Additionally, bright luminescence, high quantum efficiencies, and very low thermal quenching of these Eu^{2+}-doped borohydrides show that such host materials could serve in solid state lighting applications.

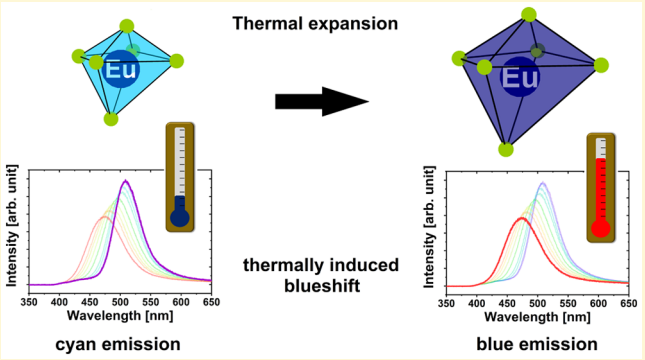

INTRODUCTION

Applications of rare earth-doped inorganic materials are manifold, ranging from solid state lighting to scintillators, lasers, biomedical applications, multiphoton processes, temperature sensing, quantum information technology, and many more.[1−11] Especially the $4f^{n-1}5d-4f^n$ transitions of Eu^{2+} (n = 7) and Ce^{3+} (n = 1) are of great importance for phosphors used in phosphor-converted light-emitting diodes (pc-LEDs).[1,4,12,13] They usually show high emission intensities and also a strong dependence of the emission energy on the host material. While Eu^{2+} and Ce^{3+} emission in a number of host materials ranging from halides to nitrides has been studied for some time,[14−16] hydride, borohydride, and mixed anionic hydrides have only been considered as host lattices recently.[17]

For instance, the hydride perovskites $LiMH_3$ and $LiMD_3$ (M = Sr, Ba) doped with Eu^{2+} have been thoroughly studied using luminescence, thermoluminescence, electron paramagnetic resonance, and electron nuclear double resonance spectroscopy.[18−22] In particular, well-resolved vibrational fine structures of the Eu^{2+}-based emission bands are observable in these compounds, and in the binary hydrides MH_2 (M = Ca, Sr, Ba) it was shown that the high polarizability of the hydride anion leads to the hitherto largest red shifts of the energies of the lowest excited $4f^65d^1$ electronic levels among all known inorganic host compounds.[23] Besides ionic hydrides, also Eu^{2+}-doped borohydrides and mixed-anionic hydrides have been studied lately.

A general finding is that in borohydrides the emission energies of the Eu^{2+}-based $4f^65d^1-4f^7$ emission so far are rather comparable with those observed typically in halides. For instance, broad blue luminescence and a quantum yield of 75% was reported for $[Eu(BH_4)_2(THF)_2]$,[24] and different shades of blue were also reported for an Eu^{2+}-related emission in the perovskite-analogue borohydrides $RbEu(BH_4)_3$, CsEu-

Received: July 30, 2019
Revised: October 6, 2019
Published: October 7, 2019

DOI: 10.1021/acs.chemmater.9b03048
Chem. Mater. 2019, 31, 8957−8968

$(BH_4)_3$, or $CsCa(BH_4)_3$:Eu^{2+}.[25,26] On the other hand, recently, particular interest has grown on mixed anionic hydrides. In those compounds, the Eu^{2+}-based emission energies strongly depend on the type and number of anions other than hydride. Examples for various classes of compounds are hydride fluorides,[27−29] hydride chlorides,[30,31] hydride oxide chlorides,[32] and even silicate hydrides.[33] In oxide hydrides, only luminescence of trivalent terbium and europium ions has been investigated so far.[34]

In this work, we present the luminescence properties of the Eu^{2+}-doped strontium borohydride chloride $Sr(BH_4)_{2-x}Cl_x$:Eu^{2+} and the alkaline metal strontium borohydride chlorides $ASr(BH_4)_{3-x}Cl_x$:Eu^{2+} (A = K, Rb, Cs) for the first time. All discussed ternary compounds show efficient cyan emission at room temperature as well as a strongly temperature-dependent shift of the emission energies. This unusually strong response of the luminescence properties of Eu^{2+} with regard to temperature changes may be interesting for potential applications in the field of thermometry.

EXPERIMENTAL SECTION

Synthesis. Due to moisture and air sensitivity all compounds were handled in an argon-filled glovebox. The mixed metal borohydrides $ASr(BH_4)_{3-x}Cl_x$:Eu^{2+} (A = K, Rb, Cs) were prepared via mechanochemical reaction of $LiBH_4$ (Alfa Aesar, 95%), $SrCl_2$ (Alfa Aesar, 99.995%), the corresponding alkaline borohydrides (KBH_4, Alfa Aesar 98%); $RbBH_4$ and $CsBH_4$ prepared from Rb or Cs metal and $NaBH_4$ in ethanol according to the procedure described in ref 35 as well as EuH_2 (2 mol % doping; synthesized via hydrogenation of europium metal in an autoclave made from hydrogen-resistant Böhler L718 alloy) in a Fritsch Pulverisette Premium Line 7 in a ZrO_2 bowl with an overpressure valve. $Sr(BH_4)_{2-x}Cl_x$:Eu^{2+} was prepared via mechanochemical reaction of stoichiometric amounts of $SrCl_2$, $LiBH_4$, and 2 mol % EuH_2. Ten ZrO_2 balls with a diameter of 10 mm are used together with approximately 0.3 g of reactants. Caution! Overpressure may build up during milling via decomposition of the borohydrides. Reactants were milled during 19 cycles with 2 min of milling at 600 rpm followed by 3 min pauses to prevent heating of the samples. To increase crystallinity, the samples were annealed at 200 °C in fused silica ampules for 2 days.

Powder X-ray Diffraction (XRD). For powder XRD analysis, a STOE STADI P diffractometer (Cu $K\alpha_1$ radiation, λ = 1.54051 Å (determined from a silicon standard), Ge-(111)-monochromator) including a DECTRIS Mythen 1 K detector was used. Samples were enclosed in 0.3 mm glass capillaries. Data was collected in the range of 2θ = 10−100° within 2 h. Structural analysis was performed with the program package Topas V5[36] and the fundamental parameter approach.[37] Cell parameters, atomic positions of the metal atoms, hydrogen and chlorine content, thermal displacement parameters, zero shift, background, size, and strain parameters were refined. For more details of the refinement process the reader is referred to Table S2 in the Supporting Information.

Temperature dependent XRD patterns from 140 to 290 K with intermediate steps of 25 K were recorded on a STOE IPDS 2T single crystal diffractometer in powder acquisition mode with Mo-radiation (λ = 0.71073 Å). Samples were prepared in 0.3 mm capillaries and measured over 3 min per "temperature step" with an imaging plate distance of 200 mm resulting in a diffraction range of 2θ = 4°−35°.

Luminescence Spectroscopy. Due to moisture and air sensitivity, all samples were enclosed in silica ampules (5 mm diameter).

Photoluminescence excitation spectra at room temperature were recorded using a xenon plasma lamp (Energetic eq 99X) with a Jobin-Yvon HR 250 monochromator (1200 grooves/mm) for excitation and an Acton Spectra Pro 2150 dual grating monochromator together with a Pixis 100 CCD camera for detection. Photoluminescence excitation and emission spectra at 4.2 K were acquired with a Xenon arc lamp (450 W) and an Edinburgh FLS920 spectrofluorometer with a single 0.25 m monochromator combined with appropriate band-pass and long pass filters. Emission was detected with a Hamamatsu R928 photomultiplier tube (PMT). The samples were cooled with an Oxford Instruments liquid He flow cryostat with external temperature control unit. All emission spectra were corrected for the wavelength-dependent PMT sensitivity and monochromator light output while excitation spectra were corrected for the reference signal of the Xe lamp.

Temperature-dependent photoluminescence emission measurements were carried out from 14 to 490 K in a Sumitomo Cryogenics HC-4E closed-cycle cryostat with a Lakeshore 340 temperature controller. A xenon lamp (Energetic eq 99X) was used as the excitation source, and spectra were recorded using an Acton Spectra Pro 2150 dual grating monochromator (300 grooves/mm, 550 nm center wavelength) and a Princeton Instruments PI 100 CCD camera. The samples were attached to a coldfinger with the aid of silver paint and copper tape.

Quantum yields were measured on a Hamamatsu Quantaurus-QY Absolute PL quantum yield spectrometer equipped with a 150 W xenon light source, a Czerny-Turner type spectroscope, and a Spectralon coated Ulbricht sphere. Ampules containing borohydrides were opened prior to the measurements, and powders were transferred immediately to the integrating sphere for measurements.

Thermal Analysis (DSC). The differential scanning calorimetry (DSC) measurements were carried out using a Netzsch DSC 200 F3Maja calorimeter in the temperature range from 295 to 673 K and nitrogen atmosphere with heating and cooling rates of 10 K/min. Approximately 5 mg of the samples were loaded into aluminum crucibles and sealed with a press (Netzsch).

RESULTS AND DISCUSSION

Synthesis and Crystal Structure. The alkaline metal strontium borohydride chlorides $ASr(BH_4)_{3-x}Cl_x$ (A = K, Rb, Cs) were obtained from the mechanochemical metathesis reaction of lithium borohydride, the alkaline metal borohydride, and strontium chloride according to the following equation:

$$2LiBH_4 + ABH_4 + SrCl_2 \rightarrow ASr(BH_4)_{3-x}Cl_x + (2 - x)LiCl + xLiBH_4 \quad (1)$$

with A = K, Rb, or Cs. For Eu^{2+}-doped samples, EuH_2 was added (2 mol %). Mechanochemical metathesis reactions of this kind are a well-known tool for the synthesis of mixed-anion and mixed-cation borohydrides.[26,38−41]

$ASr(BH_4)_{3-x}Cl_x$ (A = K, Rb, Cs) crystallize in perovskite-related orthorhombic structures as reported before for the pure borohydrides $ASr(BH_4)_3$ (A = K, Rb, Cs) by Møller et al.[42] In $ASr(BH_4)_3$ (A = K, Rb, Cs) the Sr^{2+} ions are surrounded by six $[BH_4]^-$ tetrahedra, forming a distorted octahedron. These octahedra are connected via corners to build up a three-dimensional network. The structure of $KSr(BH_4)_3$ is shown in Figure 1 (for A = Rb, Cs see Figure S1 in the Supporting Information). All three compounds share the same structural motif. Due to the similar ionic radii of Sr^{2+} and Eu^{2+},[43] it can be expected that Eu^{2+} occupies the strontium site and is therefore coordinated by a distorted octahedron of $[BH_4]^-$ units.

Table 1 summarizes selected structural information for $ASr(BH_4)_{3-x}Cl_x$ (A = K, Rb, Cs) and $Sr(BH_4)_{2-x}Cl_x$ obtained from Rietveld refinement. A detailed list of the atomic positions is given in the Supporting Information, Table S1.

For the chloride content x, 0.20, 0.14, and 0.26 were obtained for A = K, Rb, and Cs, respectively. The partial chloride substitution in mixed metal borohydrides prepared by mechanochemical milling is in good agreement with previously reported works.[26,40] Exemplarily, the Rietveld refinement of the structure of $KSr(BH_4)_{2.80}Cl_{0.20}$ is shown in Figure 2. Additional Rietveld refinements of the structures of $Sr(BH_4)_{1.74}Cl_{0.26}$,

DOI: 10.1021/acs.chemmater.9b03048
Chem. Mater. 2019, 31, 8957−8968

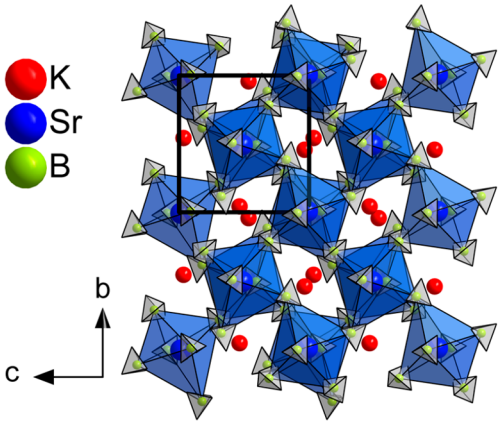

Figure 1. Representative crystal structure of $KSr(BH_4)_3$ according to ref 42. Sr (blue) is coordinated by six $[BH_4]^-$ tetrahedra (gray) building up a three-dimensional network. Hydrogen atoms of the $[BH_4]^-$ units are omitted for clarity.

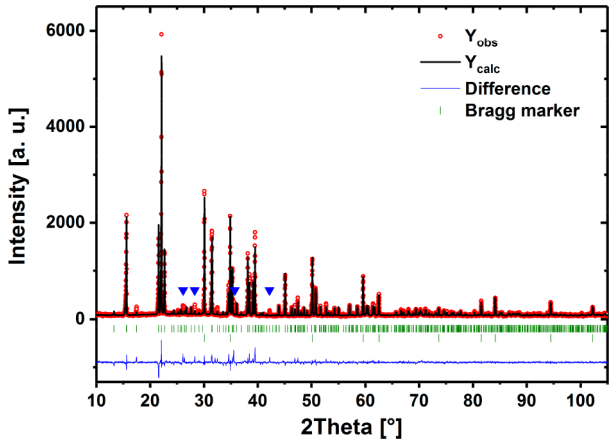

Figure 2. Rietveld refinement of $KSr(BH_4)_{3-x}Cl_x$. Structural refinement yields a substitution of $[BH_4]^-$ units with Cl^- of $x = 0.20$. After ball milling, approximately 32 wt % of LiCl is obtained as a secondary phase, and blue triangles mark a nonidentifiable phase. Bragg markers from top to bottom: $KSr(BH_4)_{2.80}Cl_{0.20}$, LiCl.

$RbSr(BH_4)_{2.86}Cl_{0.14}$, and $CsSr(BH_4)_{2.74}Cl_{0.26}$ are compiled in Figures S2–S4 of the Supporting Information.

$Sr(BH_4)_{1.74}Cl_{0.26}$:Eu^{2+} was obtained from the mechanochemical reaction of $SrCl_2$ with two equivalents of $LiBH_4$ and 2 mol % EuH_2 for Eu^{2+}-doping as reported by Ravnsbæk et al.[40] $Sr(BH_4)_2$ crystallizes orthorhombically in space group *Pbcn*, and Sr is coordinated by six $[BH_4]^-$ units, which form a slightly distorted octahedron.

For $KSr(BH_4)_{2.80}Cl_{0.20}$, a DSC measurement showed no phase transition in the range of −160 to 250 °C (see Figure S14 in the Supporting Information). At 252 °C, an endothermic signal indicates the decomposition at much lower temperatures compared to the pure borohydride analogue $KSr(BH_4)_3$ reported by Møller et al.,[42] which decomposes at approximately 400 °C. Møller et al. suggested that, at 258 °C, a structural transformation to a HT-polymorph of $KSr(BH_4)_3$ occurs. The authors came to that conclusion based on additional reflections observed in high temperature synchrotron diffraction patterns. Yet, in their DSC measurements they did not observe any heat flow changes in the corresponding temperature range, only a strong endothermic signal at 400 °C. The borohydride chloride $KSr(BH_4)_{2.80}Cl_{0.20}$ presented in this work, in turn, does not show any strong signal at 400 °C, but it does at significantly lower temperature (252 °C), which suggests decomposition as also confirmed by ex situ XRD. For samples that were heated to 250 and 300 °C, respectively, XRD analysis showed two phases of $KSr(BH_4)_{3-x}Cl_x$ with different x values at 250 °C (see Figure S5 in the Supporting Information). At 300 °C, the sample clearly darkened and only one $KSr(BH_4)_{3-x}Cl_x$ phase is present. After treatment at 400 °C, the powder appeared black, which suggests a decomposition of the remaining phase at higher temperatures.

Temperature-dependent crystal structure data from X-ray powder diffraction patterns collected on a single crystal diffractometer from 140 K to room temperature showed a temperature dependence of the lattice parameters for the mixed metal borohydride chlorides $ASr(BH_4)_{3-x}Cl_x$ (A = K, Rb, Cs) (see Figures S6–S13 in the Supporting Information). In the range between room temperature and 600 K, DSC and ex situ X-ray diffraction were used (see Figures S14 and S5, respectively, in the Supporting Information). For all ions A, an increase of temperature results in a linear increase of the cell parameters. Accordingly, positive volumetric thermal expansion coefficients can be deduced, namely, 14.5×10^{-5} K^{-1} (A = K), 9.2×10^{-5} K^{-1} (A = Rb), and 6.9×10^{-5} K^{-1} (A = Cs) according to eq 2,

$$\alpha_V = \frac{1}{V}\left(\frac{\partial V}{\partial T}\right)_p \tag{2}$$

where the subscript indicates constant (ambient) pressure conditions. The magnitude of the thermal expansion coefficient is particularly related to the anisotropy in different bonds within a given crystal or, alternatively, the increasing degree of anharmonicity of the respective collective vibrations. According to the crystal structure data of the pure ternary borohydrides, the decreasing magnitude from A = K to A = Cs also becomes readily

Table 1. Crystallographic Information for the Mixed Metal Borohydrides $ASr(BH_4)_{3-x}Cl_x$ (A = K, Rb, Cs) and $Sr(BH_4)_{2-x}Cl_x$

	compound			
	$KSr(BH_4)_{3-x}Cl_x$	$RbSr(BH_4)_{3-x}Cl_x$	$CsSr(BH_4)_{3-x}Cl_x$	$Sr(BH_4)_{2-x}Cl_x$
space group	$P2_1cn$ (No. 33)	$Pbn2_1$ (No. 33)	$P22_12_1$ (No. 18)	*Pbcn* (No. 60)
cell parameters [Å]				
a	11.3749	8.2717	6.0840	6.9160
b	8.3074	8.0830	8.0941	8.3096
c	7.5106	11.5538	8.0867	7.5129
d(Sr–B) [Å]	2.71–3.54	2.38–3.65	2.84–3.24	2.96–3.13
d_{avg}(Sr–B) [Å]	3.06 ± 0.12	3.00 ± 0.17	3.01 ± 0.06	3.02 ± 0.08
CN (Sr)	6	6	6	6
x (via Rietveld)	0.20	0.14	0.26	0.26

DOI: 10.1021/acs.chemmater.9b03048
Chem. Mater. 2019, 31, 8957–8968

evident upon already regarding the coordination sphere of the Sr^{2+} ions as a representative example: the coordination spheres of the $[Sr(BH_4)_6]^{4-}$ octahedra become less distorted upon variation of A = K to A = Cs. This critical point will be reviewed in terms of its effects on the photoluminescence properties of Eu^{2+} below in detail.

Luminescence Spectroscopy. After short milling times of only 90 min at 600 rpm the Eu^{2+}-doped samples already exhibit intense cyan luminescence in mixed cationic borohydride chlorides and blue in Sr borohydride chloride under UV excitation (Figure 3).

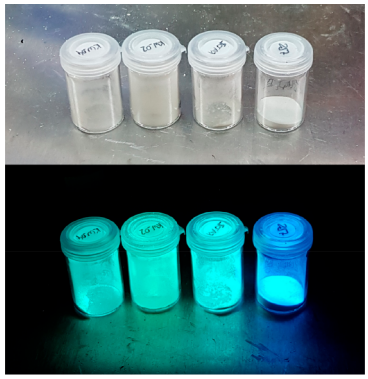

Figure 3. Photographs of $ASr(BH_4)_{3-x}Cl_x$ (A = K, Rb, Cs; x = 0.20, 0.14, 0.26) and $Sr(BH_4)_{2-x}Cl_x$ (x = 0.26) from left to right. Top: Samples under daylight. Bottom: Samples under 365 nm excitation in an argon filled glovebox.

Figure 4 depicts the photoluminescence excitation and emission spectra of $ASr(BH_4)_{3-x}Cl_x$ (A = K, Rb, Cs; x = 0.20, 0.14, 0.26) at 4.2 K and room temperature after having annealed the samples at 200 °C for 2 days. All three Eu^{2+}-activated ternary borohydride compounds show a broad emission located in the cyan range at around 490−500 nm. The broad banded appearance of the emission is typical for the parity-allowed $4f^65d^1$−$4f^7$ transition of Eu^{2+}. Similar emission spectra have been previously recorded by Schouwink et al.[25,26] in the mixed borohydrides $CsCa(BH_4)_3$:Eu^{2+} and $CsEu(BH_4)_3$ that were also prepared by mechanochemical synthesis. Another example is the molecular compound $[Eu(BH_4)_2(THF)_2]$ reported by Marks et al.[24] In contrast, there is only the corresponding chloride analogue $CsSrCl_3$:Eu^{2+} reported to show the respective $4f^65d^1 \rightarrow 4f^7$ emission transition at around 431 nm.[44,45]

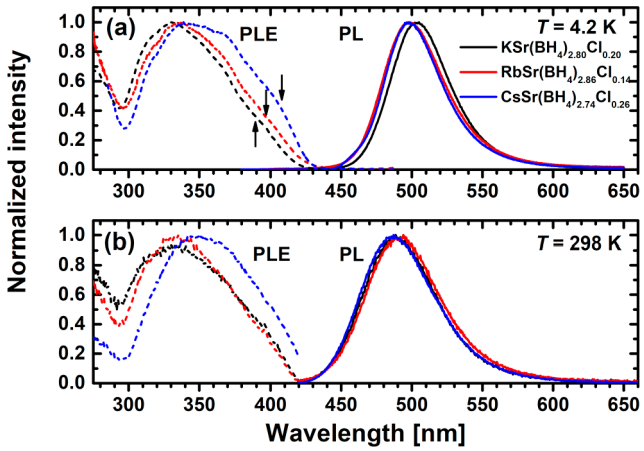

Figure 4. (a) Photoluminescence excitation (dashed) and emission spectra (solid) of Eu^{2+} in $ASr(BH_4)_{3-x}Cl_x$ (A = K, Rb, Cs; x = 0.20, 0.14, 0.26) at 4.2 K (b) same measurements at room temperature. For λ_{ex} and λ_{em} of the respective spectra, see Table 2. The arrows mark the estimated positions of the emissive $4f^6(^7F_0)5d^1$ states.

Since Rietveld analyses result in low chloride substitution for the here reported mixed anionic alkaline metal strontium borohydride chlorides the photoluminescence properties originate mainly from the borohydride ligands, and as will also be argued below, the Cl^- ligands only have a negligible effect thereon.

The maxima in the photoluminescence excitation spectra of these compounds are systematically red-shifted from K (330 nm) over Rb (335 nm) to Cs (339 nm) and exhibit a broadened fine structure both at 4.2 K and room temperature (see Figure 4a,b, dashed lines). The fine structure is typically argued to be related to the underlying spin−orbit splitting of the $4f^6$ core into the different ^7F_J (J = 0, ..., 6) levels in the excited $4f^65d^1$ configuration. It should be noted, however, that this is only a valid interpretation scheme if the Coulomb and isotropic exchange interactions between the $4f^6$ core and the 5d electron are negligibly small compared to the crystal field and spin−orbit coupling interaction. Yanase and Kasuya[46] or Weakliem[47] have shown that a fine structure can, however, also be explained taking this interaction explicitly into account. Both came to the conclusion that the dominant intensities stem from transitions of the $^8S_{7/2}$ ground level to the still almost spin-pure octet-based Kramers' doublets. Strongly ionic compounds such as fluorides, borates, or halides[48,49] often exhibit a yet well-resolved fine structure that would not be readily expected based on the stronger interaction between the 4f and the 5d electrons. Typically, this is related to the high symmetry and the related largely retained degeneracy of many of the crystal field states that supports a good resolution. In contrast, more covalent host compounds often tend to show less resolved fine structure in the excitation spectra, although an almost negligible 4f−5d Coulomb exchange interaction is expected for these cases based on the expanded 5d orbitals by means of the nephelauxetic effect. This limited resolution in the presented borohydride chlorides even at 4.2 K is a result of several consequences. Strong electron−phonon coupling induced by the more polarizable BH_4^- ions in addition to symmetry distortions from octahedral symmetry have a counteracting effect on the resolution of spectra and lead to severe homogeneous broadening effects. In addition, the presence of Cl^- impurities in the presented compound may additionally affect local symmetries and may lead to inhomogeneous broadening such that the overall resolution of the spectra is low.

The gradual red shift of the excitation maximum from the K- to Cs-based compound may be asserted by a repulsive effect of the second coordination sphere on the Eu^{2+} ions and, thus, counteracting destabilization of the excited $4f^65d^1$ configuration. Since K^+ ions are smaller than Rb^+ and Cs^+ ions, the former may approach the Eu^{2+} ions more closely.[43] The alike positive charge then leads to a repulsive contribution, which in turn destabilizes the $4f^65d^1$ configuration and should in total induce a higher energy of that configuration in the K-based compound compared to the energy in the Cs-based compound. This interpretation is additionally suggested by various longer and more anisotropic Sr−B bond lengths in the ground state structure of the K representative compared to the Cs representative (see also Table 1 and Figure 5).

DOI: 10.1021/acs.chemmater.9b03048
Chem. Mater. 2019, 31, 8957−8968

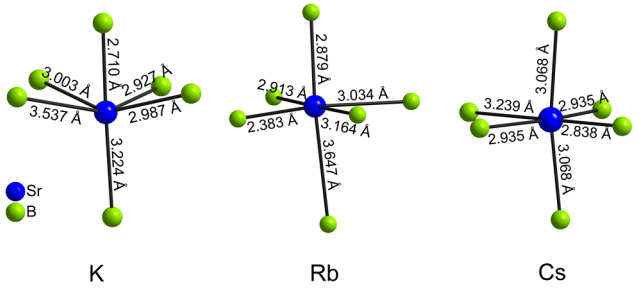

Figure 5. Bond lengths of the three ternary strontium borohydride chlorides in the respective $[Sr(BH_4)_6]$ octahedra. The structural anisotropies of the octahedra decrease from K over Rb to Cs. Hydrogen atoms are omitted for clarity.

In line with the consequences of such a repulsive impact, excitation from a very localized and shielded $4f^7$ configuration of Eu^{2+} to a more open or covalent $4f^65d^1$ configuration should induce a higher degree of excited state relaxation in the K-based compound to allow the ligand field to minimize its energy with respect to this higher degree of Coulomb repulsion. Thus, it is expected that the bond length in the excited $4f^65d^1$ configuration changes more strongly for A = K than for A = Cs. This is in line with the observed trend of Stokes shifts (see Table 2). Due to the higher number of different excited states underlying the broad excitation bands of Eu^{2+}, an accurate determination of the Stokes shift for this divalent lanthanide ion is far from trivial and typically only approximately possible. Based on the positions of the zero-phonon lines (ZPLs) determined by the crossing point between emission and excitation spectra at 4.2 K (see Figure 4a), the Stokes shifts may be approximated by twice the energy difference between the ZPL and the emission maximum (see also discussion on the Huang–Rhys–Pekar factors below). This approximation affords the values of $\Delta S = 5600\ cm^{-1}$, $5140\ cm^{-1}$, and $4800\ cm^{-1}$ for A = K, Rb, and Cs, respectively. Besides the expected decreasing trend from A = K to Cs and the connected successive symmetrization of the coordination sphere of Eu^{2+}, these values reasonably assess the position of the emissive $4f^6(^7F_0)5d^1$ state assuming a valid interpretation of the decoupled interaction scheme between 4f and 5d electrons (see arrows in Figure 4a) as the lowest energetic shoulders of the broad excitation bands.

Another measure for the nonradiative relaxation in the excited $4f^65d^1$ configuration is the emission bandwidth of the corresponding $4f^65d^1 \rightarrow 4f^7$ transition. In contrast to the Stokes shift, it can be accurately determined over the whole temperature range between 4.2 K to around 500 K and is often in the same order of magnitude as the Stokes shift. For the considered Eu^{2+}-activated borohydride chlorides, the corresponding full widths at half-maximum (fwhm's) read $1970\ cm^{-1}$ for A = K, $2085\ cm^{-1}$ for A = Rb, and $1940\ cm^{-1}$ for A = Cs (see also Table 2). Interestingly, the Eu^{2+}-related emission band fwhm in the Rb representative is larger than in the other two compounds, which is a consequence of inhomogeneous broadening induced by the largest anisotropy of the Eu–B bond lengths in the first coordination sphere among all presented borohydride chlorides (see Table 1 and Figure 5). Thus, the emission band fwhm's reflect the local structural anisotropies around the Eu^{2+} ions more accurately than the Stokes shifts do.

For a discussion of the structure–luminescence relationship of Eu^{2+}, the emission spectra of Eu^{2+} at 4.2 K have to be regarded (see Figure 4a, solid lines). The emission maxima shift from 504 nm for A = K over 499 nm for A = Rb to 497 nm for A = Cs to systematically higher energies. This behavior is also in agreement with the previous discussion on the variation of the excitation energies and Stokes shifts. At room temperature, the emission bands of all three chloride borohydrides display a thermally induced blue shift and thereby strongly overlap (see Figure 4b).

Only the emission spectrum of Eu^{2+} in $CsSr(BH_4)_{2.74}Cl_{0.26}$ at 4.2 K displays a weakly resolved vibrational fine structure at the higher energy side. The lacking resolution may be partially attributed to the presence of the Cl^- ions that induce inhomogeneous broadening effects but also the covalent Eu-BH_4 bonds. Apart from that impact, however, the regularity in trends from both the excitation and emission spectra indicate that the Cl^- ligands do not have a significant effect on the appearance of the luminescence spectra of the presented compounds and most of the Eu^{2+} ions may be coordinated by solely $[BH_4]^-$ anions. Nonetheless, the decreasing Stokes shift from A = K to Cs relates to a correspondingly decreasing Huang–Rhys–Pekar parameter S_{eff} that serves as a measure for the strength of the electron–vibrational coupling and denotes the average number of vibrations emitted during the relaxation process.[50] It can be estimated from the emission spectra by comparison of the integrated intensity I_0 of the zero-phonon transition (being estimated by the crossing point between emission and excitation spectra) relative to that of the vibrational sidebands, I_p,[50]

$$I_0 = I_p e^{-S_{eff}} \tag{3}$$

It should be noted that due to the different nature of the chemical bond in the $4f^7$ ($^8S_{7/2}$) and $4f^65d^1$ electronic states, respectively, also the Huang–Rhys–Pekar factors for the excitation transition and emission transition then differ, respectively. S_{eff} is then the geometric mean of these two values and a reliable effective measure, especially if it is small. Based on eq 3, the values for S_{eff} for the different chloride borohydrides may be estimated (errors ~ ±0.3) as $S_{eff} = 6.3$ (A = K), $S_{eff} = 5.6$ (A = Rb), and $S_{eff} = 5.0$ (A = Cs). Although the estimated values

Table 2. Characteristic Optical Parameters Deduced from the Photoluminescence Spectra of $ASr(BH_4)_{3-x}Cl_x$ (A = K, Rb, Cs; x = 0.20, 0.14, 0.26)[a]

	excitation maximum		emission maximum		zero phonon line (ZPL)		fwhm	Stokes shift	decay time[c]
compound	[nm]	[cm^{-1}][b]	[nm]	[cm^{-1}][b]	[nm]	[cm^{-1}][b]	[cm^{-1}][b]	[cm^{-1}][b]	[ns]
$KSr(BH_4)_{2.80}Cl_{0.20}$	330	29690	504	19830	436	22630	1970	5600	608
$RbSr(BH_4)_{2.86}Cl_{0.14}$	335	29130	499	19990	438	22565	2085	5140	598
$CsSr(BH_4)_{2.74}Cl_{0.26}$	339	27270	497	20000	444	22400	1940	4800	558

[a]Values refer to 4.2 K if not noted otherwise. [b]Obtained by proper conversion of the photon counts per constant wavelength interval into wavenumber domain by inclusion of the factor $\left|\frac{d\tilde{\nu}}{d\lambda}\right| = \frac{1}{\lambda^2}$. [c]Values refer to room temperature.

DOI: 10.1021/acs.chemmater.9b03048
Chem. Mater. 2019, 31, 8957–8968

of the different Huang−Rhys−Pekar factors should not be considered as very accurate based on the weakly resolved vibronic fine structure only, the difference between the Huang−Rhys−Pekar factors is significant. This is noteworthy given the fact that the alkali ions only reside in the second coordination sphere of Eu^{2+} and, thus, illustrate the yet sensitively detectable local response of the Eu^{2+}-based luminescence thereon. Additionally, a lower effective Huang−Rhys−Pekar parameter should give better resolved vibrational fine structure, which is in agreement with the observations on $CsSr(BH_4)_{2.74}Cl_{0.26}$ (cf. Figure 4a).

From the Huang−Rhys−Pekar factors S_{eff} and the determined Stokes shifts ΔS (see Table 2), an average value for the vibrational mode that is coupled to an electronic transition is estimated by the high fwhm limit[51]

$$\Delta S = 2S_{eff}\hbar\omega_{eff} \quad (4)$$

and gives an average value of $\hbar\omega_{eff} = (460 \pm 10)\ cm^{-1}$ among the three Eu^{2+}-activated ternary chloride borohydrides. This value agrees very well with the observed highest energetic librational mode in the pure borohydride perovskites $ACa(BH_4)_3$[25,52] and also fits to the expectation that the electronic states of Eu^{2+} should couple to a vibrational mode that also influences the Eu−B bonds instead of internal vibrational modes of the $[BH_4]^-$ units themselves. In particular, the relevance of this librational mode for the anharmonic structural phase transitions in the pure borohydrides was emphasized.[52] Furthermore, the photoluminescence decay curves at room temperature have been recorded for $ASr(BH_4)_{3-x}Cl_x:Eu^{2+}$ (Supporting Information Figures S16−S19 and Table 2). In all compounds, the Eu^{2+}-based emission intensity shows a single exponential decay, and lifetimes of about 608 ns for $KSr(BH_4)_{2.80}Cl_{0.20}$, 598 ns for $RbSr(BH_4)_{2.86}Cl_{0.14}$, and 558 ns for $CsSr(BH_4)_{2.74}Cl_{0.26}$ were obtained. This is in reasonable agreement with decay times reported for the Eu^{2+} emission in metal hydrides,[17] fluorides,[53] or other complex oxides[54] at room temperature. Lifetimes found in hydrides and borohydrides are usually somewhat shorter than in other classes of materials, like halides or oxides, at comparable energies. A possible explanation might be the different refractive index, which has a strong influence on the radiative decay rate.[55] Due to the higher polarizability of hydrides, one might expect the refractive index to be higher than, for instance, in some oxides, and this will lead to a faster radiative decay. Comparingly, the here reported lifetimes are shorter than the values reported for the pure halides $CsMBr_3$ and $CsMI_3$ (M = Mg, Ca, Sr) at room temperature, which are in the range of around 800−900 ns at room temperature instead.[48,49] This variation is attributed to an impact of nonradiative decay, which correlates with the vibrational energies of the local modes or phonons that the electronic states of the Eu^{2+} ions couple to. The vibrational coupling energy in the presented borohydride chlorides at around 460 cm^{-1} is right in between the maximum phonon energies found in fluorides or several complex oxides between 350 cm^{-1} and 700 cm^{-1},[56] thus explaining the similarity in the respective decay times of the $4f^65d^1$ configuration at room temperature. In contrast, the phonon energies of bromides and iodides are in the range of 160 cm^{-1} to 120 cm^{-1},[57] and as a result, the corresponding $4f^65d^1$-related decay times become slightly longer. An additional influence stems from photonic effects on the radiative decay time such as the refractive index, inducing a local field correction in a dielectric, but also the emission wavelength (λ_{em}^{-3} dependence of the Einstein coefficient of spontaneous emission).[58] These effects become, however, only clearly distinguishable at very low temperatures when nonradiative decay is negligible.

Temperature dependent luminescence emission spectra of Eu^{2+} have been recorded for all ternary chloride borohydrides and are shown in Figure 6. While all compounds are

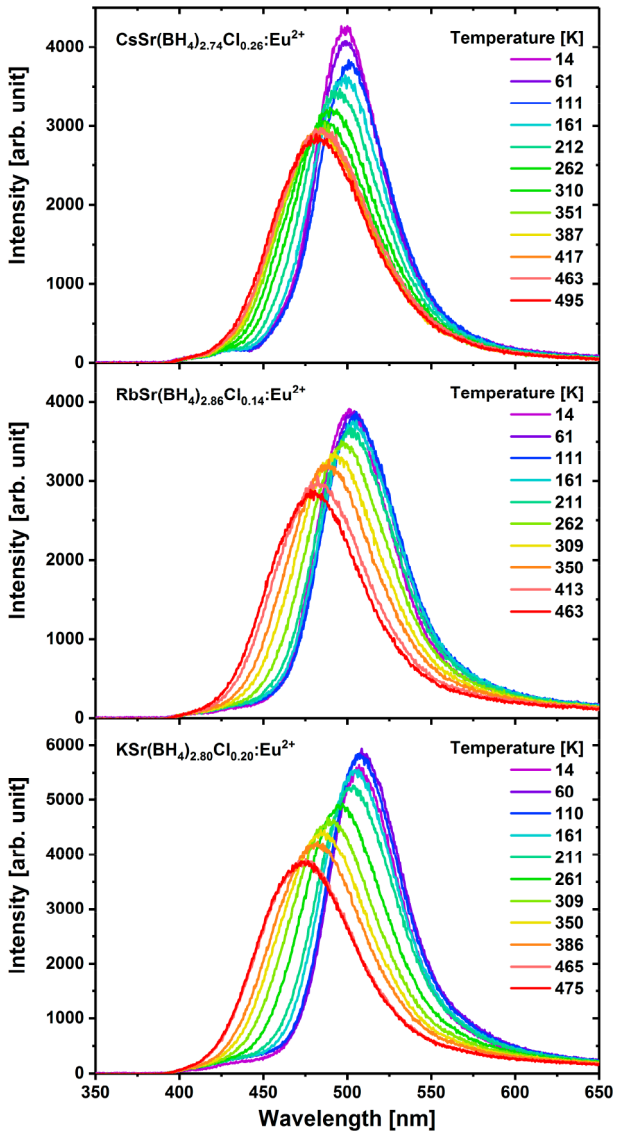

Figure 6. Temperature dependent photoluminescence spectra of the $4f^65d^1 \rightarrow 4f^7$ transition of Eu^{2+} in $CsSr(BH_4)_{2.74}Cl_{0.26}$ (top, λ_{ex} = 350 nm), $RbSr(BH_4)_{2.86}Cl_{0.14}$ (middle, λ_{ex} = 330 nm), and $KSr(BH_4)_{2.80}Cl_{0.20}$ (bottom, λ_{ex} = 330 nm) excited with a xenon lamp.

characterized by a vibrationally induced broadening of the emission bands (see also Figure S23 for the temperature evolution of the full widths at half-maximum), the integrated emission intensity remains very stable even up to 500 K (decrease by less than 10%, see Figures S20−S22) and indicates that despite the potentially high energetic stretching vibrations of the $[BH_4]^-$ ligands at around 2400 cm^{-1},[52] quenching of the Eu^{2+} luminescence in the chloride borohydrides is inefficient. Decomposition of the borohydrides hinders further recording of luminescence spectra above 500 K. However, the present data clearly suggest that the quenching temperature $T_{50\%}$ should be well above 500 K for A = K, Rb, and Cs (see Figures S20−S22 of the Supporting Information).

DOI: 10.1021/acs.chemmater.9b03048
Chem. Mater. 2019, 31, 8957−8968

Since all reported Eu^{2+}-doped compounds show very intense photoluminescence even up to 500 K, internal quantum yield measurements at room temperature were carried out to determine the efficiency of these phosphors. Table 3 compares the quantum yield for Eu^{2+} emission on $ASr(BH_4)_{3-x}Cl_x$ (A = K, Rb, Cs) with previously reported quantum yields in similar compounds.

Table 3. Absolute Quantum Yield (QY) of Different Eu-Containing Borohydride Compounds at 293 K

compound	λ_{exc} [nm]	λ_{ems} [nm]	quantum yield [%]
$KSr(BH_4)_{2.80}Cl_{0.20}:Eu^{2+}$	330	489	93
$RbSr(BH_4)_{2.86}Cl_{0.14}:Eu^{2+}$	330	492	53
$CsSr(BH_4)_{2.74}Cl_{0.26}:Eu^{2+}$	350	486	76
$[Eu(BH_4)_2(THF)_2]$[23]	360	490	75
$[Eu(BH_4)(THF)_5][BPh_4]$[23]	360	458	5

Among the mixed metal borohydride chlorides $ASr(BH_4)_{3-x}Cl_x$ (A = K, Rb, Cs), the highest efficiency is found for A = K with 93% internal quantum yield followed by Cs (76%) and Rb (53%). For comparison, Marks et al. reported an absolute quantum yield of 75% for $[Eu(BH_4)_2(THF)_2]$ and was able to increase the quantum yield to 93% by deuteration of the compound.[24]

In addition to the previously characterized features of the temperature-dependent luminescence of Eu^{2+}, an extraordinary blue shift of the $4f^65d^1 \rightarrow 4f^7$-related emission maxima with increasing temperatures is observed in all three ternary mixed borohydrides $ASr(BH_4)_{3-x}Cl_x$ (see Figure 6), and this observation remains unchanged after repeated heating and cooling steps. As depicted in Figure 7, the Eu^{2+}-based

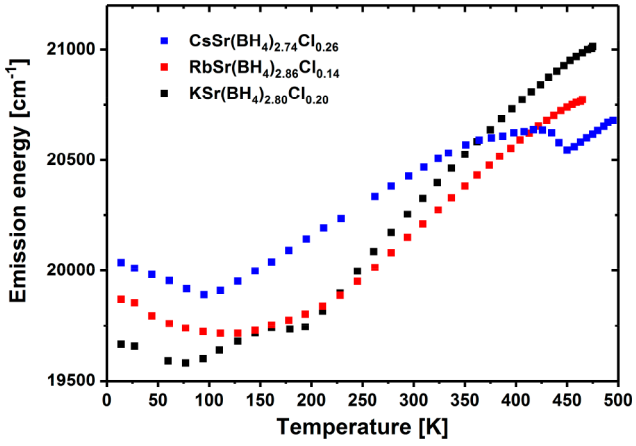

Figure 7. Temperature dependent peak maximum of the Eu^{2+} photoluminescence emission in $ASr(BH_4)_{3-x}Cl_x:Eu^{2+}$ (A = K, Rb, Cs; x = 0.20, 0.14, 0.26).

luminescence in all three compounds first displays a slight red shift within the range of 15 to 150 K, while a blue shift emerges at higher temperatures. The net blue shift of the temperature-dependent emission maxima systematically decreases from ΔE_{em} = 1500 cm^{-1} for A = K over ΔE_{em} = 990 cm^{-1} for A = Rb to ΔE_{em} = 700 cm^{-1} for A = Cs between 14 and 495 K. This feature is perfectly correlated to the trend of thermal expansion coefficients as derived from the temperature-dependent XRD measurements and indicates that the Eu^{2+}-based luminescence sensitively reacts on the successively anisotropically increasing bond lengths from 140 K on (see Figures S9, S11, and S13).

The temperature-dependent peak maxima for A = K, Rb, and Cs are shown as a function of temperature in Figure 7.

Predictions of the direction and magnitude of the temperature-dependent shifts of the emission maxima in, e.g., Eu^{2+}- and Ce^{3+}-activated phosphors are not always straightforward. Yan[59] proposed that one reason for the observation of a red shift can be the broadening of the emission band with increasing temperature, which may lead to an increased self-absorption due to a larger overlap of the photoluminescence excitation and emission spectra.

A blue shift, on the other hand, can have several origins. One important cause is lattice expansion, which increases the activator−ligand distance and, thus, results in a smaller crystal field splitting and decreasing covalency of the lanthanide−ligand bond. Furthermore, thermally induced population of higher vibrational states may lead to a higher emission energy with increasing temperature due to the presence of hot vibrational side bands. For approximately harmonic vibronic states, however, it was shown that thermal population of the higher vibrational states does not affect the energetic position of the emission maximum.[51]

In addition, also the thermal excitation into the energetically closely lying spin−orbit ^7F_J levels (J = 1, 2) of the $4f^6$ core of the excited configuration may induce a systematic blue shift and has been interpreted to occur in other Eu^{2+}-activated halides before.[48] However, given the energy difference of only 400 cm^{-1} between the $^7F_0$ and $^7F_1$ level in the $4f^6$ core,[60] this mechanism alone cannot be responsible for the significantly strong thermochromic blue shift of the Eu^{2+}-based emission observed in these mixed anionic borohydrides (see Figure 6) in the range between 1000 and 1500 cm^{-1} in all three compounds. Upon comparison to conventionally observed thermochromic blue shifts of the $4f^65d^1 \rightarrow 4f^7$ configuration of Eu^{2+} in other host compounds[48,49] on the order of only ∼100 cm^{-1}, the presented borohydride chlorides are unique in their thermal Eu^{2+}-related photoluminescence response. For instance, such compounds could, in principle, be used as internal temperature sensors in in situ neutron diffraction studies where transparent reaction chambers are used.[61] Certainly, this would probably require additional pressure calibration due to the dependence of the emission on the interatomic distances and the related vibrational modes. Further options could be the encapsulation into a polymer matrix to overcome air and moisture sensitivity in the future and using the particles in reaction monitoring under different atmospheres as is currently investigated for various processes for other phosphors with temperature-dependent peak positions.[62] Due to decomposition of the $KSr(BH_4)_{2.80}Cl_{0.20}:Eu^{2+}$ at higher temperatures, no luminescence emission could be studied above 500 K. The steady and sensitive blue shift as a response to external temperature changes in the region between 200 and 475 K combined with the fact that this mixed anionic borohydride does not decompose in this temperature region under atmospheric inert gas pressure or under hydrogen atmosphere make especially this compound a promising local and sensitive temperature sensor, for example, during hydrogenation reactions, as will also be quantitatively assessed below.

As the $4f^65d^1$ configuration reacts sensitively to local structural changes in the coordination environment of the Eu^{2+} ions, we propose the following mechanistic explanation for the large temperature induced blue shift. At low temperatures,

DOI: 10.1021/acs.chemmater.9b03048
Chem. Mater. 2019, 31, 8957−8968

the bond lengths between Eu^{2+} (being as large as Sr^{2+}) and the surrounding $[BH_4]^-$ units are highly anisotropic, which give rise to a deviation from perfect octahedral symmetry of the coordination sphere of the Eu^{2+} ions. Correspondingly, the lowest energetic emissive $4f^65d^1(t_{2g})$ crystal field states of Eu^{2+} will lose their degeneracy and split up into at most three states. Since the smaller K^+ ions in the second coordination sphere may approach closer to the Eu^{2+} ions than the bulkier Rb^+ and Cs^+ ions, the Eu−B bonds in the first coordination sphere increase from the Cs to the K compound on average (see also Table 1 and Figure 5). In turn, the low symmetry splitting of the 5d orbitals of Eu^{2+} should decrease from $CsSr(BH_4)_{2.74}Cl_{0.26}$ over $RbSr(BH_4)_{2.86}Cl_{0.14}$ to $KSr(BH_4)_{2.80}Cl_{0.20}$ due to the overall increasing bond lengths in that order. Correspondingly, any excitation from the shielded $4f^7$ to the chemically more covalent $4f^65d^1$ configuration will affect the bond length most in the A = K-related representative, which is additionally accompanied by large Stokes shifts. This explains the energetic order of the $4f^65d^1 \rightarrow 4f^7$-based emission bands at low temperatures (see Figure 4a).

If the temperature is raised, the collective vibrational motion of the host crystal (including the local coordination sphere of the Eu^{2+} ions) systematically makes the Eu−B bonds more isotropic in thermal average. Correspondingly, at some temperature, the octahedral symmetry is approximately retained and the $4f^65d^1(t_{2g})$ levels recover their degeneracy. In agreement with that picture, the emission should be systematically blue shifted and can cover larger energy difference dependent on the symmetry-induced splitting of the t_{2g} states, in agreement with observations. Alternatively, the thermally induced lattice expansion should generally increase the Eu−B bonds on average and, thus, lead to a generally observable blue shift of the Eu^{2+}-related emission with increasing temperature in all three compounds. A strong indication for the relevance of vibrations for the photoluminescence properties of these compounds is given by the different magnitudes of blue shifts among the three ternary borohydride chlorides. Their values are in perfect line with the decreasing size of the thermal expansion coefficients α_V from A = K to A = Cs (see above and Figures S9, S11, and S13). As the thermal expansion coefficient is an indirect measure for the response of a crystal to thermally excited (in particular, anharmonic) vibrations, and it is also expected that the A = K representative should show the largest blue shift of the Eu^{2+}-related emission. In turn, that also implies that, at a certain temperature, the three compounds should emit at around the same wavelength, which is in fact the case at around room temperature (see Figure 4b or 7). At higher temperatures, it is then expected that the emission energies reverse their order and that the A = K should show the most blue shifted emission, also in agreement with observations.

The observed red shifts of the Eu^{2+}-based $4f^65d^1 \rightarrow 4f^7$ emission in all compounds $ASr(BH_4)_{3-x}Cl_x$ (see Figure 7) at temperatures below 150 K may be easily explained in the framework of this model if α_V is negative at those temperatures. Future studies are already ongoing to verify both this aspect and also the applicability of this model in other related compounds. Another impact can be the balance between thermally induced vibrational broadening of the emission and corresponding symmetrization of the coordination sphere around Eu^{2+} at higher temperatures. In fact, the full widths at half-maximum (fwhm's) of particularly the Rb- and Cs-based compound increase almost linearly with temperature even below 150 K, while in the K-based compound, the Eu^{2+}-based emission fwhm remains constant at those temperatures (see Figure S23 in the Supporting Information). A hint on the validity of this balancing interpretation is the vanishing of the blue shift of the $4f^65d^1 \rightarrow 4f^7$ emission of Eu^{2+} in $KSr(BH_4)_{2.80}Cl_{0.20}$ in exactly the temperature range of constant fwhm's.

Compared to well-established classes of host materials for phosphors such as oxides, borohydride hosts illustratively show the very large temperature-dependent shifts of the $4f^65d^1 \rightarrow 4f^7$ emission energies of Eu^{2+} by tailoring the local environment, which makes them potentially good candidates to investigate temperature-dependent phenomena and also for a new class of temperature sensors.

The emission energies and europium−ligand distances found in the present work are subsequently compared to similar compounds with octahedrally coordinated europium/strontium sites and different anions reported earlier and can be seen in Table 4.

Table 4. Various Europium-Doped Strontium Compounds with the Coordination Number (CN = 6), Their Emission Wavelengths, and Atomic Distances $d(Sr-X)$[a]

compound	$d(Sr-X)$ [Å]	$d_{avg}(Sr-X)$ [Å]	emission [nm]	ref
$SrSO_4$	3.40−3.95	3.57	378	63
$SrLiB_9O_{15}$	3.33−3.90	3.68	385[c]	64
$Sr_3(PO_4)_2$	3.44	3.44	413[d]	65
$Sr_3P_4O_{13}$	3.25−3.82	3.48	415[e]	66
$CsSrBr_3$	3.05−3.08	3.06	428−430	48, 67
$CsSrI_3$	3.36	3.36	446−454	49, 68
$NaSrPO_4$	3.20−4.15	3.67	451	69
$[Eu(BH_4)(THF)_5][BPh_4]$	[b]	[b]	458	24
$Eu(BH_4)_2$	[b]	[b]	465	25
$Sr(BH_4)_{1.74}Cl_{0.26}$	2.96−3.14	3.02	457	this work
$CsEu(BH_4)_3$	[b]	[b]	485	25
$CsCa(BH_4)_3$	[b]	[b]	485	25
$CsSr(BH_4)_{2.74}Cl_{0.26}$	2.84−3.24	3.01	486	this work
$KSr(BH_4)_{2.80}Cl_{0.20}$	2.71−3.54	3.06	488	this work
$[Eu(BH_4)_2(THF)_2]$	[b]	[b]	490	24
$[Eu(BD_4)_2(THF)_2]$	[b]	[b]	490	24
Sr_2SiO_4	3.15−4.22	3.79	490[d]	70
$RbSr(BH_4)_{2.86}Cl_{0.14}$	2.38−3.65	3.00	492	this work
SrSe	3.12	3.12	564	71
$LiSr_4[BO_3]_3$	3.26	3.26	588[d]	72
SrS	3.01	3.01	620	73
SrO	2.61	2.61	625	74

[a]The given atomic distances in compounds with simple anions correspond to the europium−anion distance, whereas in compounds with complex anions, the distances are given as distances between europium and the central atom of the complex anion. [b]Not reported. [c]$[BO_4]_5$ units [d]Second polyhedron with CN other than 6. [e]Second and third polyhedrons with CN other than 6.

Combined with the high quantum yields and thermally stable luminescence, the Eu^{2+}-activated chloride borohydrides may be considered as potential luminescent thermometers. The vast majority among the currently still developed luminescent thermometers work with luminescence intensity ratios as those signals are stable toward absolute uncertainties of the intensity but merely depend on relative intensity uncertainties

DOI: 10.1021/acs.chemmater.9b03048
Chem. Mater. 2019, 31, 8957−8968

only. In contrast, the most prominent thermal response of the presented three chloride borohydrides $ASr(BH_4)_{3-x}Cl_x:Eu^{2+}$ (A = K, Rb, Cs) is the emission band shift. A figure of merit for the performance of a luminescent thermometer is the relative sensitivity, which relates its thermal response to the corresponding signal at a given temperature.[75,76] Specifically, it reads for any band shift

$$S_r(T) = \left| \frac{1}{E_{em}} \frac{\partial E_{em}}{\partial T} \right| = \left| \frac{1}{\lambda_{em}} \frac{\partial \lambda_{em}}{\partial T} \right| \quad (5)$$

with E_{em} and λ_{em} as the emission energy or wavelength at temperature T, respectively. It should be explicitly mentioned that the relative sensitivity is invariant with respect to the chosen quantity for the emission position (E_{em} and λ_{em}). The relative sensitivity readily allows different thermometers to be compared irrespective of their underlying operating principle. With eq 5, maximum relative sensitivities of $S_r = 2.85 \times 10^{-2}$ %·K^{-1} for A = K (at 245 K), $S_r = 2.12 \times 10^{-2}$ %·K^{-1} for A = Rb (at 324 K), and $S_r = 1.51 \times 10^{-2}$ %·K^{-1} for A = Cs (at 178 K) were derived. Given the commonly observed blue shifts of an Eu^{2+}-related emission of around 100 cm^{-1} between 10 and 300 K,[48,49,77,78] the relative sensitivities of the $4f^65d^1 \rightarrow 4f^7$ emission in the chloride borohydrides are about 1 order of magnitude larger and, thus, make these compounds unique among Eu^{2+}-activated phosphors in the context of the thermal emission band position response. It is noteworthy that they are even competitive to the reported relative thermal sensitivities of CdSe quantum dots ($S_r = 1.59 \times 10^{-2}$ %·K^{-1}) using the temperature-dependent emission position shift as a response signal,[79,80] while detection of the peak shift of a Nd^{3+}-based $4f^3(^4F_{3/2}, R_2) \rightarrow 4f^3(^4I_{11/2}, Z_1)$ emission transition in the crystal field of $ALa(PO_3)_4$ (A = Li−Rb) was shown to act an order of magnitude more sensitively ($S_r = 0.48\%\cdot K^{-1}$).[81]

In contrast, however, the absolute temperature-dependent luminescence intensity or fluorescence decay time of CdSe[82−84] or, more recently, Ag_2S quantum dots[85,86] has been shown to react by orders of magnitude more sensitively ($S_r > 2\%\cdot K^{-1}$) to small temperature changes. Also, the usage of a luminescence intensity ratio of two emission bands using lanthanides as emitters has already been shown to respond more sensitively to small temperature changes (even $S_r > 10\%\cdot K^{-1}$) in various temperature regimes.[76,87−91] The reader is referred to several excellent reviews on that topic for a broad overview of this quickly emerging field.[92−96] Thus, although the presented Eu^{2+}-activated chloride borohydrides $ASr(BH_4)_{3-x}Cl_x$ (A = K, Rb, Cs) are very sensitive in terms of their temperature-dependent emission band position, detection of the emission maximum as itself does not provide the thermal relative sensitivities already achievable in practical luminescent thermometers. This circumstance is related to the type of detected temperature response (energy or wavelength shift) itself being much lower than the reference signal (energy or wavelength). It is, however, similarly possible to quantify the blue shift by means of an analogous ratiometric area analysis. By integration of the low- and high-energy side of the temperature-dependent emission spectra (see Figures S28 and S29 in the Supporting Information), which mimics the usage of corresponding bandpass filters, it is possible to achieve an alternative quantification for the blue shift. A similar operating principle is used by ratio pyrometers that detects the emitted blackbody radiation of any object at two different wavelengths. If R denotes the ratio between the integrated intensity of the high-energy portion I_2 and low-energy portion I_1, the corresponding relative sensitivity may be given by

$$S_r(T) = \left| \frac{1}{R} \frac{\partial R}{\partial T} \right| \quad (6)$$

The thus obtained relative thermal sensitivities are much higher and read $S_r = 0.91\%\cdot K^{-1}$ for A = K (at 211 K), $S_r = 0.66\%\cdot K^{-1}$ for A = Rb (at 278 K), and $S_r = 0.83\%\cdot K^{-1}$ for A = Cs (at 229 K). In fact, they are even competitive with conventional ratiometric thermometers ($S_r \geq 1\%\cdot K^{-1}$) using two emission transitions from thermally coupled excited states.[92−97] In that sense, the presented compounds are also promising single-band luminescent thermometers.

Properties of $Sr(BH_4)_{1.74}Cl_{0.26}:Eu^{2+}$. In addition to the ternary strontium borohydride chlorides, the binary compound can be synthesized in the same manner. After ball milling of 2 equiv of $LiBH_4$ with $SrCl_2$ (2 mol % EuH_2) the blue emitting phosphor $Sr(BH_4)_{1.74}Cl_{0.26}:Eu^{2+}$ is obtained, and its photoluminescence emission spectrum reveals a broad emission band with a maximum at 457 nm at room temperature (see Figure S15 in the Supporting Information). Rietveld refinement, crystallographic information, photoluminescence excitation, and decay measurements can be viewed in the Supporting Information. Similar to the ternary compounds, a high quantum yield of 82% is achieved.

Expectedly, the bond lengths in the binary compound $Sr(BH_4)_{1.74}Cl_{0.26}$ are more isotropic and generally shorter due to the lack of a repulsive alkali cation and thus, the coordination sphere of Eu^{2+} is closer to a perfect octahedral symmetry. Accordingly, a more blue shifted excitation band compared to the presented ternary representatives should be expected due to the recovery of degenerate $4f^65d^1(t_{2g})$ crystal field states, as is also observed (*cf.* Figure S15 in the Supporting Information). A similar model was already presented to explain the difference between the photoluminescence of Eu^{2+} in the iodides $CsCaI_3$ compared to $CsMgI_3$ and $CsSrI_3$, respectively.[49]

CONCLUSION

The mixed metal borohydride chlorides $ASr(BH_4)_{3-x}Cl_x$ (A = K, Rb, Cs) and $Sr(BH_4)_{1.74}Cl_{0.26}$ have been synthesized by mechanochemical reaction. These borohydride hosts show very efficient luminescence at room temperature upon doping with 2 mol % europium and very low thermal quenching. All mixed metal borohydride chlorides show thermally induced significant shifts of the emission energies and also a unique sensitivity toward local changes even in the second coordination sphere. In addition, the $4f^65d^1 \rightarrow 4f^7$ emission of the Eu^{2+}-activated ternary chloride borohydrides shows thermally induced blue shifts on the order of 1000 to 1500 cm^{-1} so far never observed for Eu^{2+} to the best of our knowledge, which makes them promising candidates for temperature sensing applications in a relevant temperature regime (200 K−500 K), e.g., for the in situ studies of hydrogenation reactions. Despite the fact that the relative thermal sensitivity of this blue shift is below the much better optimized ratiometric or luminescence decay time thermometers, it is competitive to even quantum dot-based thermometers with the same operating principle of a thermally induced change in emission position.

The unusual temperature-dependent behavior of the emission maximum is correlated to the lattice expansion of the host and especially to the temperature-dependent behavior of the bond lengths between Eu^{2+} and the surrounding $[BH_4]^-$ units. At low

DOI: 10.1021/acs.chemmater.9b03048
Chem. Mater. 2019, 31, 8957−8968

temperatures, bond length anisotropy gives a deviation from perfect octahedral symmetry of the coordination sphere of the Eu^{2+} ions and red shifts the $4f^65d^1 \rightarrow 4f^7$ emission. Upon increasing the temperature, the collective vibrational motion of the host crystal systematically makes the Eu−B bonds more isotropic in the thermal average, leading to a recovery of the octahedral symmetry. This explanation is in good agreement with the observation that the thermal expansion coefficients α_V decrease from A = K to A = Cs, consistent with the different magnitudes of blue shifts observed for these compounds. In summary, the differences of the Eu^{2+} emission for the different compounds and their thermal behavior impressively show the potential of the optical properties of Eu^{2+} as a local structure sensor. The incorporation of these phosphors into polymer-based matrices to protect them from moisture and air should principally be feasible and will be investigated in the future with suitable polymers.

■ ASSOCIATED CONTENT

Supporting Information

The Supporting Information is available free of charge on the ACS Publications website at DOI: 10.1021/acs.chemmater.9b03048.

Additional data on the thermal shifts, X-ray studies, and lifetime measurements of the mixed metal borohydride chlorides (PDF)

■ AUTHOR INFORMATION

Corresponding Author

*(N.K.) E-mail: nathalie.kunkel@uni-goettingen.de.

ORCID

Atul D. Sontakke: 0000-0001-5132-0942
Victor Castaing: 0000-0002-8426-338X
Andries Meijerink: 0000-0003-3573-9289
Nathalie Kunkel: 0000-0002-4541-3461

Author Contributions

The manuscript was written through contributions of all authors. All authors have given approval to the final version of the manuscript.

Funding

This research was supported by a Liebig fellowship including doctoral fellowship of the Fonds der Chemischen Industrie (FCI), Grant no. Li 197/02, the German Research Foundation (DFG, KU 3427/4-1), and the Bavarian-French Academy Center for a Mobility aid (Az. FK03_2017). M.S., B.V., and A.M. acknowledge funding from the EU-FET-Open project nanoTBtech (Grant Agreement No. 801305).

Notes

The authors declare no competing financial interest.

■ ACKNOWLEDGMENTS

N.K. and T.W. would like to thank Prof. Fässler for hosting our group, P. Walke for help with DSC measurements, Dr. C. Jandl for help with quantum yield measurements, Dr. W. Klein and Dr. V. Hlukhyy for help with the temperature dependent XRD measurements, and C. Kriebisch as well as K. Weber for help with the syntheses.

■ REFERENCES

(1) Pust, P.; Weiler, V.; Hecht, C.; Tücks, A.; Wochnik, A. S.; Henß, A.-K.; Wiechert, D.; Schmidt, P. J.; Schnick, W.; Scheu, C. Narrow-band red-emitting $Sr[LiAl_3N_4]:Eu^{2+}$ as a next-generation LED-phosphor material. *Nat. Mater.* **2014**, *13*, 891.

(2) Smet, P. F.; Joos, J. J. Stabilizing colour and intensity. *Nat. Mater.* **2017**, *16*, 500.

(3) Strobel, P.; Maak, C.; Weiler, V.; Schmidt, P. J.; Schnick, W. Ultra-narrow-band blue-emitting oxoberyllates $AELi_2[Be_2O_6]:Eu^{2+}$ (AE = Sr, Ba) Paving the way to efficient RGB pc-LEDs. *Angew. Chem., Int. Ed.* **2018**, *57*, 8739.

(4) Hoerder, G. J.; Seibald, M.; Baumann, D.; Schröder, T.; Peschke, S.; Schmid, P. C.; Tyborski, T.; Pust, P.; Stoll, I.; Bergler, M.; Patzig, C.; Reißaus, S.; Krause, M.; Berthold, L.; Höche, T.; Johrendt, D.; Huppertz, H. $Sr[Li_2Al_2O_2N_2]:Eu^{2+}$ - A high performance red phosphor to brighten the future. *Nat. Commun.* **2019**, *10*, 1824.

(5) Zhou, J.; Liu, Q.; Xia, Z. Structural construction and photoluminescence tuning via energy transfer in apatite-type solid-state phosphors. *J. Mater. Chem. C* **2018**, *6*, 4371.

(6) Kolesov, R.; Xia, K.; Reuter, R.; Stöhr, R.; Zappe, A.; Meijer, J.; Hemmer, P. R.; Wrachtrup, J. Optical detection of a single rare-earth ion in a crystal. *Nat. Commun.* **2012**, *3*, 1029.

(7) Xu, J.; Murata, D.; Ueda, J.; Tanabe, S. Near-infrared long persistent luminescence of Er^{3+} in garnet for the third bio-imaging window. *J. Mater. Chem. C* **2016**, *4*, 11096.

(8) Xu, J.; Murata, D.; Katayama, Y.; Ueda, J.; Tanabe, S. Cr^{3+}/Er^{3+} co-doped $LaAlO_3$ perovskite phosphor: a near-infrared persistent luminescent probe covering the first and third biological window. *J. Mater. Chem. B* **2017**, *5*, 6385.

(9) Wegh, R. T.; Donker, H.; Oskam, K. D.; Meijerink, A. Visible Quantum Cutting in $LiGdF_4:Eu^{3+}$ Through Downconversion. *Science* **1999**, *283*, 663.

(10) Brites, C. D.; Xie, X.; Debasu, M. L.; Qin, X.; Chen, R.; Huang, W.; Rocha, J.; Liu, X.; Carlos, L. D. Instantaneous ballistic velocity of suspended Brownian nanocrystals measured by upconversion nanothermometry. *Nat. Nanotechnol.* **2016**, *11*, 851.

(11) Kunkel, N.; Goldner, P. Recent advances in rare earth doped inorganic crystalline materials for quantum information processing. *Z. Anorg. Allg. Chem.* **2018**, *644*, 66.

(12) Qin, X.; Liu, X.; Huang, W.; Bettinelli, M.; Liu, X. Lanthanide-activated phosphors based on 4f-5d optical transitions: Theoretical and experimental aspects. *Chem. Rev.* **2017**, *117*, 4488.

(13) Li, G.; Tian, Y.; Zhao, Y.; Lin, J. recent progress in luminescence tuning of Ce^{3+} and Eu^{2+}-activated phosphors for pc-LEDs. *Chem. Soc. Rev.* **2015**, *44*, 8688.

(14) Dorenbos, P. Energy of the first $4f^7 \rightarrow 4f^65d$ transition of Eu^{2+} in inorganic compounds. *J. Lumin.* **2003**, *104*, 239.

(15) Dorenbos, P. Ce^{3+} 5d-centroid shift and vacuum referred 4f-electron binding energies of all lanthanide impurities in 150 different compounds. *J. Lumin.* **2013**, *135*, 93.

(16) Höppe, H. A.; Lutz, H.; Morys, P.; Schnick, W.; Seilmeier, A. Luminescence in Eu^{2+}-doped $Ba_2Si_5N_8$: Fluorescence, thermoluminescence, and upconversion. *J. Phys. Chem. Solids* **2000**, *61*, 2001−2006.

(17) Kunkel, N.; Wylezich, T. Recent advances in rare earth-doped hydrides. *Z. Anorg. Allg. Chem.* **2019**, *645*, 137−145.

(18) Kunkel, N.; Meijerink, A.; Kohlmann, H. Bright yellow and green Eu(II) luminescence and vibronic fine structures in $LiSrH_3$, $LiBaH_3$ and their corresponding deuterides. *Phys. Chem. Chem. Phys.* **2014**, *16*, 4807.

(19) Kunkel, N.; Böttcher, R.; Pilling, T.; Kohlmann, H.; Pöppl, A. Eu^{2+}-containing luminescent perovskite-type hydrides studied by electron paramagnetic resonance. *Z. Phys. Chem.* **2016**, *230*, 931−942.

(20) Kunkel, N.; Sontakke, A. D.; Kohaut, S.; Viana, B.; Dorenbos, P. Thermally simulated luminescence and first-principle study of defect configurations in the perovskite-type hydrides $LiMH_3:Eu^{2+}$ (M = Sr, Ba) and the corresponding deuterides. *J. Phys. Chem. C* **2016**, *120*, 29414−29422.

(21) Lefevre, G.; Herfurth, A.; Kohlmann, H.; Sayede, A.; Wylezich, Th.; Welinski, S.; Duarte Vaz, P.; Parker, S. F.; Blach, J. F.; Goldner, Ph.; Kunkel, N. Phonon-electron coupling in luminescent europium doped hydride perovskites studied by luminescence spectroscopy, inelastic

DOI: 10.1021/acs.chemmater.9b03048
Chem. Mater. 2019, 31, 8957−8968

neutron scattering, and first-principle calculations. *J. Phys. Chem. C* **2018**, *122*, 10501.
(22) Wylezich, T.; Böttcher, R.; Sontakke, A.; Castaing, V.; Viana, B.; Pöppl, A.; Kunkel, N. Lanthanide ions as local probes in ionic hydrides: A pulsed Electron Nuclear Double Resonance and thermoluminescence study of Eu^{2+}-doped hydride perovskites. *J. Phys. Chem. C* **2019**, *123*, 5031.
(23) Kunkel, N.; Kohlmann, H.; Sayede, A.; Springborg, M. Alkaline-Earth Metal Hydrides as Novel Host Lattices for Eu^{II} Luminescence. *Inorg. Chem.* **2011**, *50* (13), 5873−5875.
(24) Marks, S.; Heck, J. G.; Habicht, M. H.; Oña-Burgos, P.; Feldmann, C.; Roesky, P. W. $[Ln(BH_4)_2(THF)_2]$ (Ln = Eu, Yb) - A highly luminescent material. Synthesis, properties, reactivity, and NMR studies. *J. Am. Chem. Soc.* **2012**, *134*, 16983.
(25) Schouwink, P.; Ley, M. B.; Tissot, A.; Hagemann, H.; Jensen, T. R.; Smrčok, L.; Černý, R. Structure and properties of complex hydride perovskite materials. *Nat. Commun.* **2014**, *5*, 5706.
(26) Paskevicius, M.; Jepsen, L. H.; Schouwink, P.; Černý, R.; Ravnsbæk, D. B.; Filinchuk, J.; Dornheim, M.; Besenbacher, F.; Jensen, T. R. Metal borohydrides and derivatives − synthesis, structure and properties. *Chem. Soc. Rev.* **2017**, *46*, 1565.
(27) Kunkel, N.; Kohlmann, H. Ionic mixed hydride fluoride compounds: Stabilities predicted by DFT, synthesis, and luminescence of divalent europium. *J. Phys. Chem. C* **2016**, *120*, 10506.
(28) Pflug, C.; Franz, A.; Kohlmann, H. Crystal structure and europium luminescence of $NaMgH_{3-x}F_x$. *J. Solid State Chem.* **2018**, *258*, 391.
(29) Wylezich, T.; Welinski, S.; Hoelzel, M.; Goldner, P.; Kunkel, N. Lanthanide luminescence as a local probe in mixed anionic hydrides − a case study on Eu^{2+}-doped $RbMgH_xF_{3-x}$ and $KMgH_xF_{3-x}$. *J. Mater. Chem. C* **2018**, *6*, 13006.
(30) Kunkel, N.; Rudolph, D.; Meijerink, A.; Rommel, S.; Weihrich, R.; Kohlmann, H.; Schleid, T. Green luminescence of divalent europium in the hydride chloride EuHCl. *Z. Anorg. Allg. Chem.* **2015**, *641*, 1220.
(31) Rudolph, D.; Wylezich, T.; Sontakke, A. D.; Meijerink, A.; Goldner, P.; Netzsch, P.; Höppe, H. A.; Kunkel, N.; Schleid, T. Synthesis and optical properties of the Eu^{2+}-doped alkaline-earth metal hydride chlorides $AE_7H_{12}Cl_2$ (AE = Ca and Sr). *J. Lumin.* **2019**, *209*, 150.
(32) Rudolph, D.; Enseling, D.; Jüstel, T.; Schleid, T. Crystal Structure and luminescence properties of the first hydride oxide chloride with divalent europium: $LiEu_2HOCl_2$ *Z. Z. Anorg. Allg. Chem.* **2017**, *643*, 1525.
(33) Gehlhaar, F.; Finger, R.; Zapp, N.; Bertmer, M.; Kohlmann, H. $LiSr_2SiO_4H$, an air-stable hydride as host for Eu(II) luminescence. *Inorg. Chem.* **2018**, *57*, 11851.
(34) Ueda, J.; Matsuishi, S.; Tokunaga, T.; Tanabe, S. Preparation, electronic structure of gadolinium oxyhydride and low-energy 5d excitation band for green luminescence of Tb^{3+} ions. *J. Mater. Chem. C* **2018**, *6*, 7541.
(35) Banus, M. D.; Bragdon, R. W.; Hinckley, A. A. Potassium, rubidium and cesium borohydride. *J. Am. Chem. Soc.* **1954**, *76*, 3848.
(36) Coelho, A. A. *Topas-Academic*, Version 5, General profile and structure analysis software for powder diffraction data; Bruker AXS: Karlsruhe, Germany; http://www.topas-academic.net (accessed Sept. 29, 2019).
(37) Coelho, A. A. Indexing of Powder Diffraction Patterns by Iterative Use of Singular Value Decomposition. *J. Appl. Crystallogr.* **2003**, *36*, 86.
(38) Ravnsbæk, D.; Filinchuk, Y.; Cerenius, Y.; Jakobsen, H. J.; Besenbacher, F.; Skibsted, J.; Jensen, T. R. A series of mixed-metal borohydrides. *Angew. Chem., Int. Ed.* **2009**, *48*, 6659.
(39) Grube, E.; Olesen, C. H.; Ravnsbæk, D. B.; Jensen, T. R. Barium borohydride chlorides: synthesis, crystal structure and thermal properties. *Dalton Trans.* **2016**, *45*, 8291.
(40) Ravnsbæk, D. B.; Nickels, E. A.; Černý, R.; Olesen, C. H.; David, W. I. F.; Edwards, P. P.; Filinchuk, Y.; Jensen, T. R. Novel alkali earth borohydrides $Sr(BH_4)_2$ and borohydride-chloride $Sr(BH_4)Cl$. *Inorg. Chem.* **2013**, *52*, 10877.
(41) Ley, M. B.; Boulineau, S.; Janot, R.; Filinchuk, Y.; Jensen, T. R. New Li ion conductors and solid state hydrogen storage materials: $LiM(BH_4)_3Cl$, M = La, Gd. *J. Phys. Chem. C* **2012**, *116*, 21267.
(42) Møller, K. T.; Ley, M. B.; Schouwink, P.; Černý, R.; Jensen, T. R. Synthesis and thermal stability of perovskite alkali metal strontium borohydrides. *Dalton Trans.* **2016**, *45*, 831.
(43) Shannon, R. Revised effective ionic radii and systematic studies of interatomic distances in halides and chalcogenides. *Acta Crystallogr., Sect. A: Cryst. Phys., Diffr., Theor. Gen. Crystallogr.* **1976**, *32*, 751.
(44) Gahane, D. H.; Kokode, N. S.; Bahirwar, B. M.; Moharil, S. V. Luminescence of Eu^{2+} in some chlorides. *Phys. Procedia* **2012**, *29*, 42.
(45) Cherginets, V. L.; Rebrova, N. V.; Grippa, A. Yu.; Datsko, Yu. N.; Ponomarenko, T. V.; Pedash, V. Yu.; Kosinov, N. N.; Tarasov, V. A.; Zelenskaya, O. V.; Zenya, I. M.; Lopin, A. V. Scintillation properties of $CsSrX_3:Eu^{2+}$ ($CsSr_{1-y}Eu_yX_3$, X = Cl, Br; $0 \leq y \leq 0.05$) single crystals grown by the Bridgman method. *Mater. Chem. Phys.* **2014**, *143*, 1296.
(46) Yanase, A.; Kasuya, T. Magneto-Optical Effect due to Eu^{2+} Ion. *Suppl. Progr. Theor. Phys.* **1970**, *46*, 388.
(47) Weakliem, H. A. Electronic Interactions in the $4f^6$ 5*d* Configuration of Eu^{2+} in Crystals. *Phys. Rev. B* **1972**, *6*, 2743.
(48) Suta, M.; Larsen, P.; Lavoie-Cardinal, F.; Wickleder, C. Photoluminescence of $CsMBr_3:Eu^{2+}$ (M = Mg, Ca, Sr)-A novel strategy for the development of low-energy emitting phosphors. *J. Lumin.* **2014**, *149*, 35.
(49) Suta, M.; Wickleder, C. Photoluminescence of $CsMI_3:Eu^{2+}$ (M = Mg, Ca, and Sr) − a spectroscopic probe on structural distortions. *J. Mater. Chem. C* **2015**, *3*, 5233.
(50) Huang, K.; Rhys, A. Theory of light absorption and non-radiative transitions in *F*-centres. *Proc. R. Soc. London A* **1950**, *204*, 406−423.
(51) de Jong, M.; Seijo, L.; Meijerink, A.; Rabouw, F. T. Resolving the ambiguity in the relation between Stokes shift and Huang-Rhys parameter. *Phys. Chem. Chem. Phys.* **2015**, *17*, 16959.
(52) Schouwink, P.; Hagemann, H.; Embs, J. P.; D'Anna, V.; Černý, R. Di-hydrogen contact induced lattice instabilities and structural dynamics in complex hydride perovskites. *J. Phys.: Condens. Matter* **2015**, *27*, 265403.
(53) Kobayasi, T.; Mroczkowski, S.; Owen, J. F.; Brixner, L. H. Fluorescence lifetime and quantum efficiency for 5d → 4f transitions in Eu^{2+} doped chloride and fluoride crystals. *J. Lumin.* **1980**, *21*, 247.
(54) Poort, S. H. M.; Meyerink, A.; Blasse, G. Lifetime measurements in Eu^{2+}-doped host lattices. *J. Phys. Chem. Solids* **1997**, *58*, 1451.
(55) Henderson, B.; Imbusch, G. F. *Optical Spectroscopy of Inorganic Solids*; Clarendon Press: Oxford, U.K., 1989.
(56) van Dijk, J. M. F.; Schuurmans, M. F. H. On the nonradiative and radiative decay rates and a modified exponential energy gap law for 4*f*-4*f* transitions in rare earths. *J. Chem. Phys.* **1983**, *78*, 5317.
(57) Suta, M.; Wickleder, C. Spin crossover of Yb^{2+} in $CsCaX_3$ and $CsSrX_3$ − A guideline to novel halide-based scintillators. *Adv. Funct. Mater.* **2017**, *27*, 1602783.
(58) Senden, T.; Rabouw, F. T.; Meijerink, A. Photonic effects on the radiative decay rate and luminescence quantum yield of doped nanocrystals. *ACS Nano* **2015**, *9*, 1801.
(59) Yan, S. On the origin of temperature dependence of the emission maxima of Eu^{2+} and Ce^{3+} -activated phosphors. *Opt. Mater.* **2018**, *79*, 172.
(60) Carnall, W. T.; Goodman, G. L.; Rajnak, K.; Rana, R. S. A systematic analysis of the spectra of the lanthanides doped into single crystal LaF_3. *J. Chem. Phys.* **1989**, *90*, 3443.
(61) Widenmeyer, M.; Niewa, R.; Hansen, T. C.; Kohlmann, H. In situ neutron diffraction as a probe for formation and decompositions of nitrides and hydrides: A case study. *Z. Anorg. Allg. Chem.* **2013**, *639*, 285.
(62) Abram, C.; Fond, B.; Heyes, A. L.; Beyrau, F. High-speed planar thermometry and velocimetry using thermographic phosphor particles. *Appl. Phys. B: Lasers Opt.* **2013**, *111*, 155.

DOI: 10.1021/acs.chemmater.9b03048
Chem. Mater. 2019, 31, 8957−8968

(63) Sun, J. Y.; Di, Q. M.; Han, L.; Xu, Q. G.; Ma, C. L. Hydrothermal synthesis of $SrSO_4:Eu^{2+}$ microcrystals with different morphologies and its luminescence properties. *Appl. Mech. Mater.* **2014**, *633*−*634*, 341.
(64) Diaz, A.; Keszler, D. A. Red, green, and blue Eu^{2+} luminescence in solid-state borates: A structure-property relationship. *Mater. Res. Bull.* **1996**, *31*, 147.
(65) Ji, H.; Huang, Z.; Xia, Z.; Molokeev, M. S.; Atuchin, V. V.; Fang, M.; Liu, Y. Discovery of new solid solution phosphors via cation substitution-dependent phase transition in $M_3(PO_4)_2:Eu^{2+}$ (M = Ca/Sr/Ba) quasi-binary Sets. *J. Phys. Chem. C* **2015**, *119*, 2038.
(66) Hoffman, M. V. Eu^{2+} activation in some alkaline earth strontium phosphate compounds. *J. Electrochem. Soc.* **1968**, *115*, 560.
(67) Gokhale, S. S.; Stand, L.; Lindsey, A.; Koschan, M.; Zhuravleva, M.; Melcher, C. L. Improvement in the optical quality and energy resolution of $CsSrBr_3$:Eu scintillator crystals. *J. Cryst. Growth* **2016**, *445*, 1.
(68) Yang, K.; Zhuravleva, M.; Melcher, C. L. Crystal growth and characterization of $CsSr_{1-x}Eu_xI_3$ high light yield scintillators. *Phys. Status Solidi RRL* **2011**, *5*, 43.
(69) Yim, D. K.; Song, H. J.; Cho, I.-S.; Kim, J. S.; Hong, K. S. A novel blue-emitting $NaSrPO_4:Eu^{2+}$ phosphor for near UV based white light-emitting-diodes. *Mater. Lett.* **2011**, *65*, 1666.
(70) Kim, J. S.; Park, Y. H.; Kim, S. M.; Choi, J. C.; Park, H. L. Temperature-dependent emission spectra of $M_2SiO_4:Eu^{2+}$ (M = Ca, Sr, Ba) phosphors for green and greenish white LEDs. *Solid State Commun.* **2005**, *133*, 445.
(71) Zhang, X.; Liang, L.; Zhang, J.; Su, Q. Luminescence properties of $(Ca_{1-x}Sr_x)Se:Eu^{2+}$ phosphors for white LEDs application. *Mater. Lett.* **2005**, *59*, 749.
(72) Yu, H.; Deng, D.; Hua, Y.; Li, C.; Xu, S. Orange- to green-emitting $Li(Sr,Ca)_4(BO_3)_3:Eu^{2+}$ phosphor: emission-tunable properties and white light emitting diode application. *RSC Adv.* **2016**, *6*, 82824.
(73) Xia, Q.; Batentschuk, M.; Osvet, A.; Richter, P.; Häder, D. P.; Schneider, J.; Wondraczek, L.; Winnacker, A.; Brabec, C. J. Red-emitting $Ca_{1-x}Sr_xS:Eu^{2+}$ phosphors as light converters for plant-growth applications. *Mater. Res. Soc. Symp. Proc.* **2011**, *1342*, mrss11-1342-v04-04.
(74) Yamashita, N. Photoluminescence spectra of the Eu^{2+} center in SrO:Eu. *J. Lumin.* **1994**, *59*, 195.
(75) Collins, S. F.; Baxter, G. W.; Wade, S. A.; Sun, T.; Grattan, K. T. V.; Zhang, Z. Y.; Palmer, A. W. Comparison of fluorescence-based temperature sensor schemes: Theoretical analysis and experimental validation. *J. Appl. Phys.* **1998**, *84*, 4649.
(76) Wade, S. A.; Collins, S. F.; Baxter, G. W. Fluorescence intensity ratio technique for optical fiber point temperature sensing. *J. Appl. Phys.* **2003**, *94*, 4743.
(77) ten Kate, O. M.; Xie, R.; Wang, C.; Funahashi, S.; Hirosaki, N. Eu^{2+}-Doped $Sr_2B_{2-2x}Si_{2+3x}Al_{2-x}N_{8+x}$: A boron-containing orange-emitting nitridosilicate with interesting composition-dependent photoluminescence properties. *Inorg. Chem.* **2016**, *55*, 11331.
(78) Liu, C.; Qi, Z.; Ma, C.; Dorenbos, P.; Hou, D.; Zhang, S.; Kuang, X.; Zhang, J.; Liang, H. High light yield of $Sr_8(Si_4O_{12})Cl_8:Eu^{2+}$ under X-ray excitation and its temperature-dependent luminescence characteristics. *Chem. Mater.* **2014**, *26* (12), 3709.
(79) Li, S.; Zhang, K.; Yang, J.-M.; Lin, L.; Yang, H. Single quantum dots as local temperature markers. *Nano Lett.* **2007**, *7*, 3102.
(80) Maestro, L. M.; Rodríguez, E. M.; Rodríguez, F. S.; Iglesiaz-de la Cruz, M. C.; Juarranz, A.; Naccache, R.; Vetrone, F.; Jaque, D.; Capobianco, J. A.; Solé, J. G. CdSe quantum dots for two-photon fluorescence thermal imaging. *Nano Lett.* **2010**, *10*, 5109.
(81) Marciniak, Ł.; Bednarkiewicz, A.; Hreniak, D.; Strek, W. The influence of the Nd^{3+} concentration and alkali ions on the sensitivity of non-contact temperature measurements in $ALaP_4O_{12}:Nd^{3+}$ (A = Li, Na, K, Rb) nanocrystalline luminescent thermometers. *J. Mater. Chem. C* **2016**, *4*, 11284.
(82) Walker, G. W.; Sundar, V. C.; Rudzinski, C. M.; Wun, A. W.; Bawendi, M. G.; Nocera, D. G. Quantum-dot optical temperature probes. *Appl. Phys. Lett.* **2003**, *83*, 3555.
(83) Jorge, P. A. S.; Mayeh, M.; Benrashid, R.; Caldas, P.; Santos, J. L.; Farahi, F. Quantum dots as self-referenced optical fibre temperature probes for luminescent chemical sensors. *Meas. Sci. Technol.* **2006**, *17*, 1032−1038.
(84) Cerón, E. N.; Ortgies, D. H.; del Rosal, B.; Ren, F.; Benayas, A.; Vetrone, F.; Ma, D.; Sanz-Rodríguez, F.; Solé, J. G.; Jaque, D.; Rodríguez, E. M. Hybrid Nanostructures for High-Sensitivity Luminescence Nanothermometry in the Second Biological Window. *Adv. Mater.* **2015**, *27*, 4781−4787.
(85) Santos, H. D. A.; Ruiz, D.; Lifante, G.; Jacinto, C.; Juarez, B. H.; Jaque, D. Time resolved spectroscopy of infrared emitting Ag_2S nanocrystals for subcutaneous thermometry. *Nanoscale* **2017**, *9*, 2505−2513.
(86) del Rosal, B.; Ruiz, D.; Chaves-Coira, I.; Juárez, B. H.; Monge, L.; Hong, G.; Fernandez, N.; Jaque, D. In Vivo Contactless Brain Nanothermometry. *Adv. Funct. Mater.* **2018**, *28*, 1806088.
(87) Liu, X.; Akerboom, S.; de Jong, M.; Mutikainen, I.; Tanase, S.; Meijerink, A.; Bouwman, E. Mixed-Lanthanoid Metal-Organic Framework for Ratiometric Cryogenic Temperature Sensing. *Inorg. Chem.* **2015**, *54*, 11323.
(88) Ananias, D.; Almeida Paz, F. A.; Carlos, L. D.; Rocha, J. Near-Infrared Ratiometric Luminescent Ratiometric Thermometer Based on a New Lanthanide Silicate. *Chem. - Eur. J.* **2018**, *24*, 11926.
(89) Ximendes, E. C.; Rocha, U.; Sales, T. O.; Fernández, N.; Sanz-Rodríguez, F.; Martín, I. R.; Jacinto, C.; Jaque, D. In vivo subcutaneous thermal video recording by supersensitive infrared nanothermometers. *Adv. Funct. Mater.* **2017**, *27*, 1702249.
(90) Marciniak, Ł.; Bednarkiewicz, A.; Elzbieciak, K. NIR-NIR photon avalanche based luminescent thermometry with Nd^{3+} doped nanoparticles. *J. Mater. Chem. C* **2018**, *6*, 7568.
(91) Ximendes, E. C.; Pereira, A. F.; Rocha, U.; Silva, W. F.; Jaque, D.; Jacinto, C. Thulium doped LaF_3 for nanothermometry operating over 1000 nm. *Nanoscale* **2019**, *11*, 8864.
(92) Jaque, D.; Vetrone, F. Luminescence Nanothermometry. *Nanoscale* **2012**, *4*, 4301.
(93) Brites, C. D. S.; Lima, P. P.; Silva, N. J. O.; Millán, A.; Amaral, V. S.; Palacio, F.; Carlos, L. D. *Nanoscale* **2012**, *4*, 4799.
(94) Brites, C. D. S.; Millán, A.; Carlos, L. D. Lanthanides in Luminescence Thermometry. In *Handbook on the Physics and Chemistry of Rare Earths*; Bünzli, J.-C., Pecharsky, V., Eds.; Elsevier: Amsterdam, 2016; Vol. *49*, Chapter 281, pp 339−427.
(95) Dramićanin, M. D. Sensing temperature via downshifting emissions of lanthanide-doped metal oxides and salts. A review. *Methods Appl. Fluoresc.* **2016**, *4*, No. 042001.
(96) Brites, C. D. S.; Balabhadra, S.; Carlos, L. D. Lanthanide-based thermometers: At the cutting-edge of luminescence thermometry. *Adv. Opt. Mater.* **2019**, *7*, 1801239.
(97) Errulat, D.; Marin, R.; Gálico, D. A.; Harriman, K. L. M.; Pialat, A.; Gabidullin, B.; Iikawa, F.; Couto, O. D. D., Jr.; Moilanen, J. O.; Hemmer, E.; Sigoli, F. A.; Murugesu, M. A luminescent thermometer exhibiting slow relaxation of the magnetization: Toward self-monitored building blocks for the next-generation optomagnetic devices. *ACS Cent. Sci.* **2019**, *5*, 1187.

DOI: 10.1021/acs.chemmater.9b03048
Chem. Mater. 2019, 31, 8957−8968